Defect and Diffusion Forum
ISSN: 1662-9507, Vol. 415, pp 81-99

Submitted: 2020-10-16
Revised: 2020-11-25
Accepted: 2020-11-30
Online: 2022-04-27

Experimental Investigation of Air Bubble Curtain Effects on Water Wave Field

Diogo R. C. B. Neves[1,a*], Moisés Brito[2,b], António A. Pires-Silva[3,c], Conceição J. Fortes[4,d] and Jorge Matos[3,e]

[1]Sea Technologies Group, INEGI, Campus da FEUP, Rua Dr. Roberto Frias, 400. 4200 - 465 Porto. Portugal

[2]UNIDEMI, Department of Mechanical and Industrial Engineering, NOVA School of Science and Technology, NOVA University Lisbon, 2829-516 Caparica, Portugal

[3]CERIS, Instituto Superior Técnico, Universidade de Lisboa, Av. Rovisco Pais, 1049-001, Lisboa, Portugal

[4]Harbours and Maritime Structures Division, Hydraulics and Environment Department, Laboratório Nacional de Engenharia Civil (LNEC), Av. do Brasil 101, 1700-066, Lisboa, Portugal

[a]dneves@inegi.up.pt, [b]moisesbrito@fct.unl.pt, [c]antonio.pires.silva@tecnico.ulisboa.pt, [d]jfortes@lnec.pt, [e]jorge.matos@tecnico.ulisboa.pt

Keywords: Air bubble curtain, wave propagation, flow velocities, turbulence, wave flume.

Abstract. This paper studies the effects of an air bubble curtain on surface water waves. Water particle velocities and free surface elevations were measured simultaneously at two cross-shore sections downstream the air bubble curtain. Measurements were carried out for regular waves regarding different air bubble curtain configurations. Free surface elevations were measured using resistive gauges and the instantaneous velocities were acquired using an Acoustic Doppler Velocimeter (ADV). The characteristics of the free surface elevation, velocity field and turbulence are analyzed and discussed. The free surface elevation was found to be constantly attenuated by the air bubble curtain. The phase-averaged velocity profiles also depict the effect of the air bubbles in the flow field by generating milder longitudinal velocities (u) and by increasing the transverse component of the velocity (w). The increase in the turbulence intensity and the different energy spectrum produced by the air bubble curtain is also analyzed. The experimental results indicate that the thickness of the air bubble curtain and the total air flow rate affects the wave field.

1. Introduction

The presence of air bubbles in the water column is of the utmost importance due to its effect on the water flow. In hydraulic engineering, it is known that flow aeration may lead to flow bulking, gas transfer, and energy dissipation in breaking waves. Highly aerated flows in chute spillways are characterized by drag reduction, increase of the flow velocity, and improve safety against cavitation damage [1, 2]. Furthermore, air entrainment due to wave breaking has shown to contribute both to energy dissipation and transfer of energy from short waves to long-period waves near the shoreline, which affects the sediment transport [3]. It also induces a temporary increase in water level along the surf zone [4].

Recent theoretical models, as the one from Hoque and Aoki [5], assume that entrained air bubbles first increase the potential energy of water which is dissipated during the air bubble detrainment. Horikawa and Kuo [6], Cox and Shin [7], and Mori and Kakuno [8] state that the energy dissipation is related to the turbulent air-water flows, and their work shows the relation between the entrained air quantity and the turbulent intensity. Moreover, the phenomenon contributes largely for the air-sea transfer of gases and the production of sea-salt aerosol, essential for the natural balance of the ecosystem [9].
More recently air injections on the water column establishing air bubble curtains have been studied regarding its influence on flow patterns and bed morphology in open channels and rivers. Dugué et

al. [10] performed laboratory experiments showing the potential of the air bubble screen technique to generate a secondary flow that can modify the bed morphology.

The air bubble curtains have been increasingly applied for several applications. Some companies use such technique to mitigate damage in marine environments from the noise and the effect of blasting due to mining, drilling, seismic surveys and underwater pile driving [11]. The same principle is applied to protect marine mammals and keep them away from offshore oil platforms, wind power farm construction sites and sea works with significant noise impact. This technique has also been used for fish guiding in waterways and rivers [12]. Recently, air bubble curtains have been tested at SINTEF to contain oil spills in the Trondheim Fjord in Norway [13]. An identical principle has been applied to control the motion and direction of floating debris at the island of Saint-Martin, Guadeloupe, Mexico and in Martinique [14]. In Florida, USA companies also use air bubble curtains to contain sediments in suspension [15]. Also, the air bubble technology has recently been applied to create an air bubble barrier to catch and prevent the flow of plastics. This technology not only catches the surface floating material but also the submerged debris [16].

Nowadays, it is still unclear how these air bubble curtains affect the wave field. Therefore, the study of such technology on wave field is of scientific relevance. In the present work, such effects were studied in an experimental laboratory using a 2D wave flume where propagating waves were exposed to forced air injection (air bubble curtain). This allowed the characterization of the flow with and without the air bubble curtain, quantifying its effect on the free surface elevation, velocity field, turbulence and energy dissipation. Different air bubble curtain configurations and air bubble sizes were tested. The measurements comprised free surface elevations and flow velocity profiles at two cross-shore locations downstream of the air bubble curtains.

The novel contribution of this paper is the experimental characterization of the air bubble curtain effects on water wave field. This paper first describes, in Sec. 2, the experimental setup and procedures, including the wave flume geometry, test conditions and data collection. Afterwards, the main characteristics of wave field are presented and discussed in Sec. 3. The effects of air bubble curtain configurations and air bubble sizes on the free surface elevation are presented and analyzed. The analysis is performed by phase-averaging the data in a quasi-steady condition over 120 successive wave periods. Then the velocity and turbulence fields are also analyzed using the phase-averaging technique. The effects of air bubble sizes are also discussed. The main conclusions are summarized in Sec. 4.

2. Experimental Setup

The experimental tests were conducted in a 32.4 [m] long wave flume at the National Laboratory of Civil Engineering (LNEC), Lisbon, Portugal. The wave flume length is divided by several sections. It presents a 4.8 [m] long section for wave generation, composed by a 1.3 [m] horizontal bottom and a 3.5 [m] ramp with an elevation of 0.4 [m]. After that, the bottom is characterized by a horizontal section of 11.2 [m] which is the reference of the vertical axis ($z = 0$). Afterwards the main ramp begins (reference $x = 0$ of the experiments) with a length of 9.0 [m] and a slope of 1:18. The water depth was 0.6 [m] at the horizontal section and 0.1 [m] at the top of this ramp (Fig. 1). The final section of the flume had a smooth inclined ramp with 1:136 slope with 9.53 [m] length ending with horsehair sheets and rocks to attenuate the residual wave reflection. The schematic sketch of the wave flume is shown in Fig. 1.

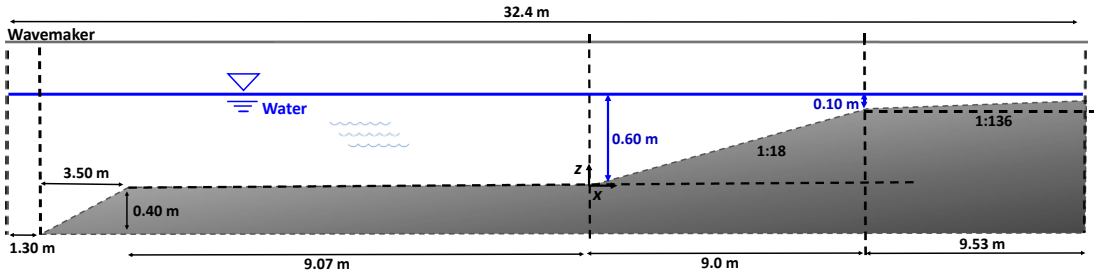

Fig. 1. Schematic sketch of the wave flume (not to scale).

The wave flume was equipped with a piston type wavemaker, led by the Labview - Signal Express® software that transferred the digital signal and converted it into voltage with a National Instruments (NI) voltage output module (NI-9263). The wavemaker presents a horizontal *x*-coordinate (longitudinal) movement and was able to generate regular waves.

An air pump with 15 W and a maximum capacity of 1200 l/h (Aqua FORTE V-20) was used to inject air in the defined sections at bottom of the flume. An Acoustic Doppler Velocimeter (ADV) and a resistive gauge were used to measure flow velocities and free surface elevations, respectively. The ADV was a Nortek® - AS VECTRINO model with a down-looking cable probe. The accuracy is 0.5% ± 0.001 m/s of the measured value and the acquisition rate was 20 Hz. The resistive gauge, manufactured at LNEC, acquired with 25 Hz frequency and with ± 0.4 mm accuracy (non-linearity is 0.5% of measuring range). Fig. 2 shows the experimental equipment.

Fig. 2. Experimental equipment: Air pump (left); Resistive gauge (centre); ADV (right).

The air injection of the bubble curtain was made by circular orifices at the bottom of the flume at section x = 3.5 [m] (Fig. 3). Both the free surface elevations and flow velocities were measured at sections x = 5.5 and 7.0 [m] (Fig. 3). The ADV measurements were performed in vertical profiles along the water column and in the middle of the horizontal transverse component of the flume (y). The vertical profiles had a 0.03 [m] distance between each measurement along the water column until the maximum z point under the wave troughs. The measurement points are depicted in Fig 3.

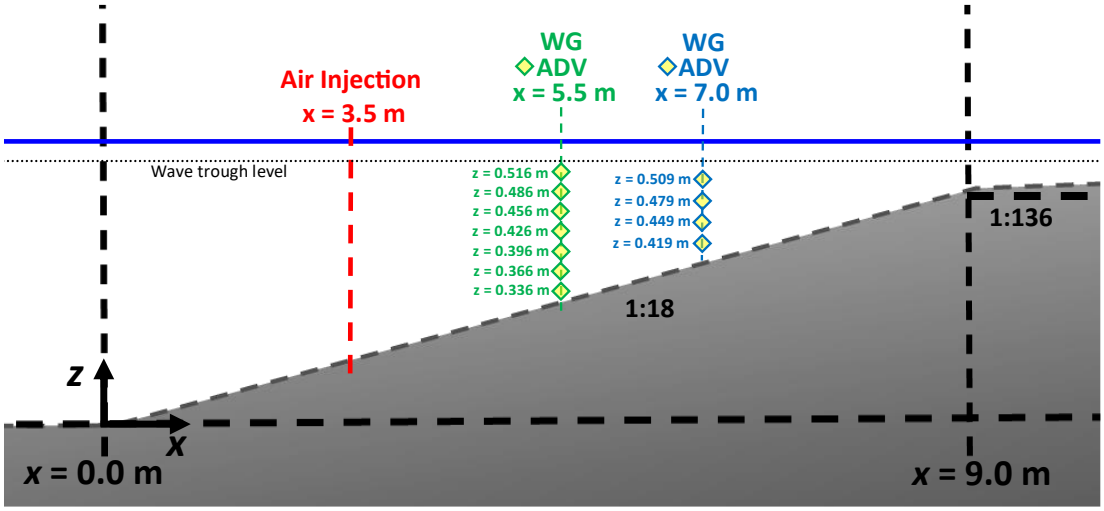

Fig. 3. Section representing the location of the air bubble curtain and the sections showing the location of both resistive wave gauge (WG) and ADV measurements.

The generated regular waves had a wave period T = 1.25 [s] and wave height of H = 0.113 [m] in the beginning of the horizontal section of the wave flume. These wave characteristics created a spilling wave breaking in the end of the 1:18 slope ramp at x = 7.5 [m]. Each test comprised 90 s of regular waves to ensure the stabilization of the wave hydrodynamics and an unchanged wave breaking section throughout the measurements. After the stabilization period, 150 regular waves were generated to be analysed and to obtain ensemble-averaged quantities. Every test was completed with a wave attenuation ramp of 90 [s]. Ting and Kirby [19] used 120 waves for phase-averaging in their experiments with regular waves.

Three different air bubble curtains were tested, namely (Fig. 4):

- Curtain ‘A’ had a space between the orifices of 0.025 [m]. In this case each orifice had a diameter of 0.002 [m] and the orifices were set at two tubes at the bottom of the flume at x = 3.475 [m] and at x = 3.525 [m].
- Curtain ‘B’ used the same size of orifices and tube configuration but had a space between orifices of 0.05 [m].
- Curtain ‘C’ was different from both other injections because it was set at just one tube at x = 3.5 [m] with a space between orifices of 0.12 [m] and an orifice diameter of 0.004 [m].

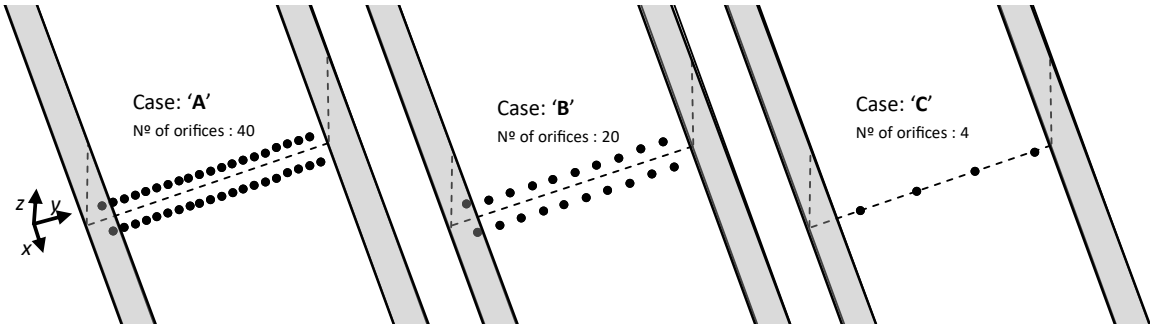

Fig. 4. Orifice configuration for the air injection in the three cases at the bottom of the wave flume: “A” (left), “B” (centre), “C” (right)

The three different types of injections covered the entire cross section of the wave flume, creating two air curtains for the ‘A’ and ‘B’ and one for ‘C’ injection. For ‘A’ and ‘B’ the tube installation required a space next to each wall of 0.05 [m] to the onset of the orifices. The wave flume at x = 3.5 [m] had 0.6 [m] width, thus the number of orifices at ‘A’ and ‘B’ was 40 and 20, respectively. The

number of orifices for the ‘C’ injection was 4. The air injected was measured at each orifice with a volumetric graduated cylinder for each air injection type (Fig. 5). An average of 5 air volume measurements was considered for each orifice.

Fig. 5. Left: Air pump and tube configuration for ‘A’ and ‘B’; Centre: tube configuration for ‘C’; Right: volumetric graduated cylinder.

Table 1 shows the orifice diameter, the space between orifices, the number of orifices, the measured average air flow rate per orifice [l/s], the total air flow rate [l/s] and the relative air bubble size considering the case C as the unit value. The relative air bubble volume was calculated as the average air flow rate per orifice of case ‘A’ or ‘B’ divided by that of case ‘C’.

Table 1. Test cases for the air injection

Case	A	B	C
Orifice diameter [m]	0.002	0.002	0.004
Space between orifices [m]	0.025	0.05	0.12
Number of orifices [m]	40	20	4
Average air rate per orifice [l/s]	0.011	0.018	0.029
Total air rate discharge [l/s]	0.440	0.369	0.116
Relative air bubble volume	0.378	0.635	1.000

The three configurations of air injections allowed comparing the effect of different air bubble curtains. Each air bubble curtain (A, B and C) discharges different quantities of air and generates different sizes of air bubbles within the curtain. Fig. 6 shows the air curtain generated for case ‘B’.

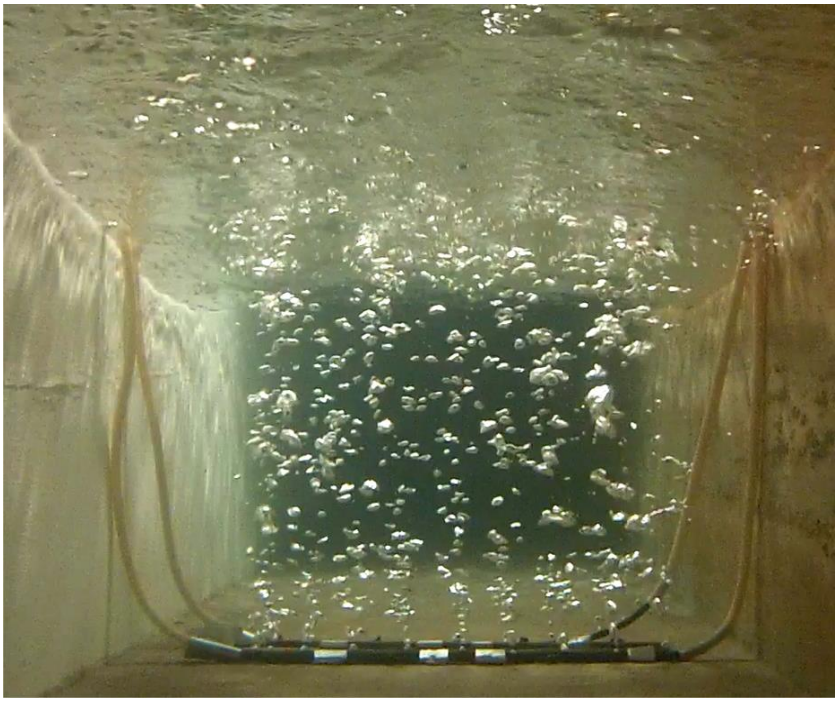

Fig. 6. Air injection at the bottom of the wave flume for case 'B'.

3. Results and Discussion

In this section, the results for the three tested cases of air bubble curtains (A, B and C) as well as for the case without air bubble curtain (NB – No Bubbles) are shown. The phase-averaging technique was applied to investigate the effects of the air bubble curtains on the wave field over a wave period. The phase-averaged of each quantity was calculated in a quasi-steady condition over 120 wave periods (see Sec. 3.1). The transient data (approximately 20 waves after the start of the wave generation) were removed from the time series analysis. The phase-average of each instantaneous quantities *F(t)* was calculated as in Cox and Shin [7], Klopman [18] and Ting and Kirby [19]:

$$\langle F(t)\rangle = \frac{1}{M}\sum_{m=0}^{M-1} F(t+mT), \qquad \text{for } t \in [0\,, T] \tag{1}$$

where *M* represents the central 120 regular waves of each test and *T* is the wave period. The turbulent fluctuation is given by:

$$F'(t) = F(t) - \langle F(t)\rangle \tag{2}$$

The root-mean-square (RMS) of turbulent fluctuation was defined as:

$$F'_{rms}(t) = \sqrt{\frac{1}{M}\sum_{m=0}^{M-1}[F(t+mT) - \langle F(t)\rangle]^2} \tag{3}$$

3.1. Free Surface Elevation. In this work, each cycle of free surface elevation and velocity is not exactly repetitive, owing to fluctuations in the order of the wave frequency regarding the overall mean periodic variation, which are an addition to the relatively small-scale high-frequency effects of the coherent structures and turbulence. A 10-wave sample of the normalized free surface elevation, η, for the case without air bubble curtain (NB), for the measured sections at x = 5.5 and x = 7.0 [m], are

presented in Fig. 7 and Fig. 8, respectively. The local water depth is represented by *h* (Fig. 1). These figures confirm that the incident wave condition presents good wave-to-wave repeatability after the quasi-steady condition.

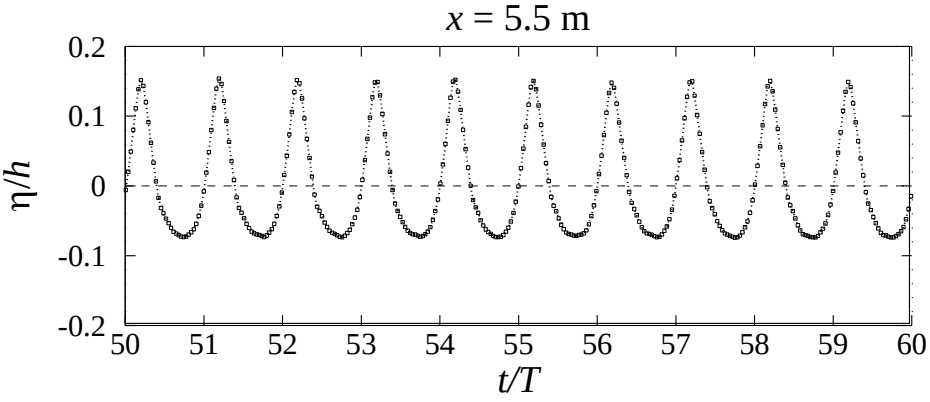

Fig. 7. Free surface elevation at section *x* = 5.5 [m] for the case NB.

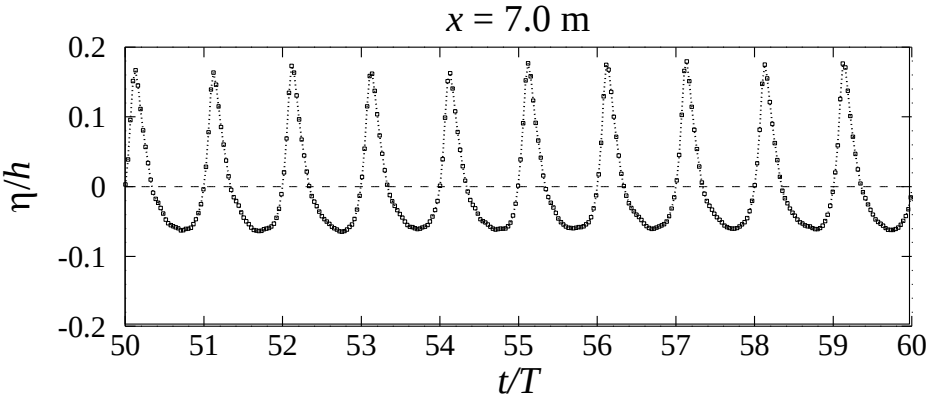

Fig. 8. Free surface elevation at section *x* = 7.0 [m] for the case NB.

Some conclusions can be drawn by applying the phase-averaging technique to the free surface elevation. Fig. 9 shows the values of $\langle\eta\rangle$ and η'_{rms} within one wave period for both sections (*x* = 5.5 and *x* = 7.0 [m]) considering all the tested air bubble curtains.

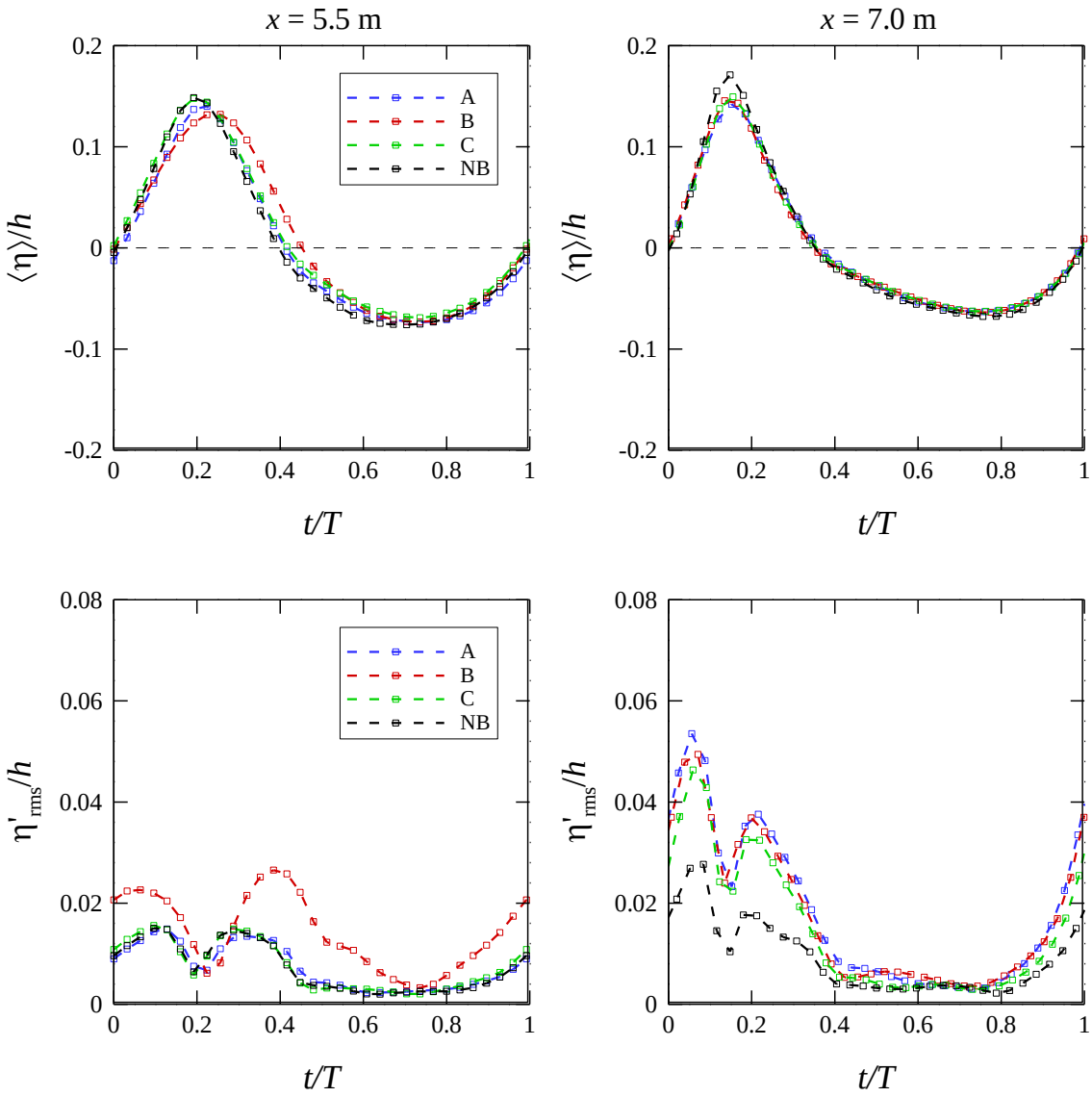

Fig. 9. Top: Phase-averaged free surface elevation along one wave period. Left: at section x = 5.5 [m]; Right: at section x = 7.0 [m]; Bottom: RMS of the averaged free surface elevation along one wave period. Left: at section x = 5.5 [m]; Right: at section x = 7.0 [m].

Fig. 9 shows, mainly for x = 7.0 [m], relevant differences between the case without air bubble curtain (NB) and the cases with the air bubble curtain (A, B and C). The $\langle\eta\rangle$ values show that for both sections (x = 5.5 and x = 7.0 [m]) the NB case presents slightly higher amplitude of $\langle\eta\rangle$ values along the wave period. At the wave crest, for section x = 5.5 [m], the average difference of $\langle\eta\rangle$ between NB and the other cases is of 0.010 [m] while, at section x = 7.0 [m], such difference is of 0.025 [m]. For x = 7.0 [m], from the wave crest until the wave trough the difference reaches 3 times η'_{rms} when comparing the case A with the NB case. Therefore, a considerable increase in the η'_{rms} for the air bubble curtain cases when comparing with the NB case. For the same section the air bubble curtain for case B follows the case A and, the case C presents a smaller effect on η'_{rms}. For section x = 5.5 [m] the η'_{rms} shows considerable differences for case B outside the wave crest and the wave trough reaching almost the double of the other cases. At this section the case without air bubble curtain do not varies much from cases A and C.

3.2. Velocity field. As mentioned before, the three components of the velocity (u, v and w) were measured with the Acoustic Doppler Velocimeter (ADV). The velocity field u, v and w stand for the longitudinal (x), transverse (y) and vertical (z) components. Fig. 10 shows a 10-wave sample of the velocity time series for the NB case regarding both longitudinal and vertical components of the

velocity, *u* and *w*, respectively. All velocity results were normalized by the deep-water particle velocity of each incident wave:

$$U_0 = \frac{\pi H}{T} \tag{4}$$

Fig. 10 reflects the vertical variability of both components of the velocity and the magnitude difference between *u* and *w*. As shown in both Fig. 7 and Fig. 8 the steepness of the wave increases 33% from *x* = 5.5 to *x* = 7.0 [m]. Such wave transformation is reflected on the time series of the velocity values (Fig. 10).

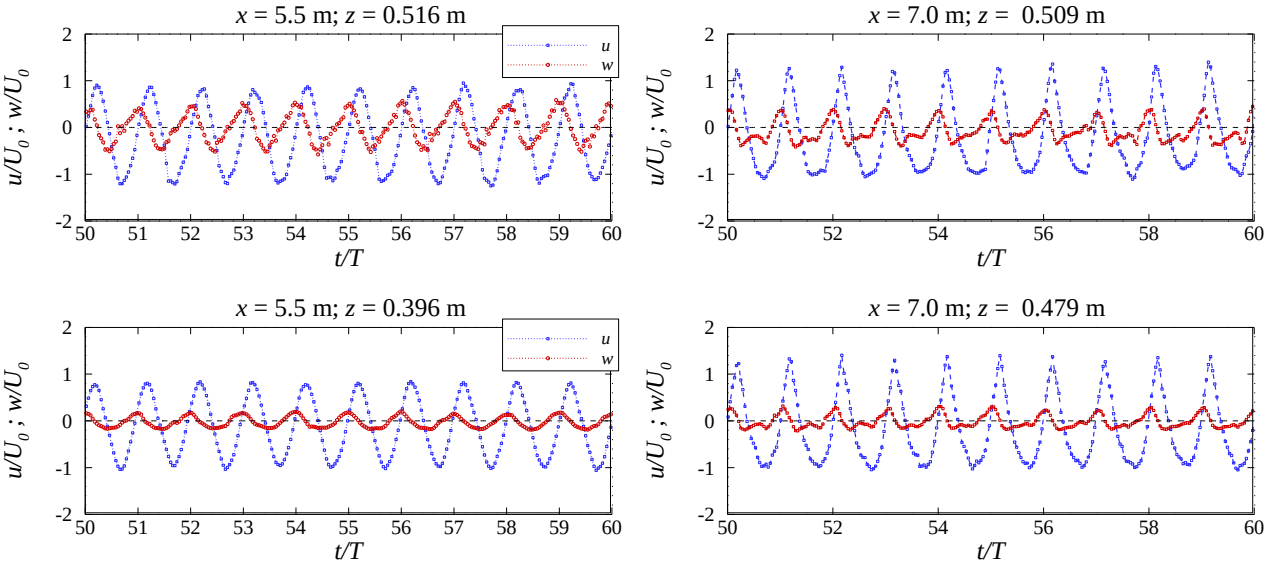

Fig. 10. Time series representing a 10-wave sample of the normalized *u* and *w* velocity components. Top-left: *x* = 5.5 and *z* = 0.516 [m]; Top-right: *x* = 7.0 and *z* = 0.509 [m]; Bottom-left: *x* = 5.5 and *z* = 0.396 [m]; Bottom-right: *x* = 7.0 and *z* = 0.479 [m].

The phase-average of the longitudinal component of the velocity (*u*) and its RMS at the closest to the free surface measuring point are shown in Fig. 11 and Fig. 12 for *x* = 5.5 and *x* = 7.0 [m], respectively.

For the point *x* = 5.5 and *z* = 0.516 [m] (Fig. 11) the u'_{rms} shows that the case of the air bubble curtain B generates the highest values, mainly at the wave crest and trough, the second and the third highest values are de ones of the air bubble curtains A and C, respectively. The case without air bubble curtain (NB) is the one that shows the lowest u'_{rms} values, except for the instants between the wave crest and the wave trough. For the w'_{rms} the same trend is observed but with less variation between cases.

Different results are observed from the velocity measurements at point *x* = 7.0 and *z* = 0.509 [m]. The u'_{rms} along one wave period shows only that at the wave crest the highest values are presented for the NB case. For w'_{rms} the case C presents the highest values along the wave period followed in the wave trough by the air bubble curtains from cases A and B. Also, for w'_{rms} the NB case is the one than presents the lower values along the wave period.

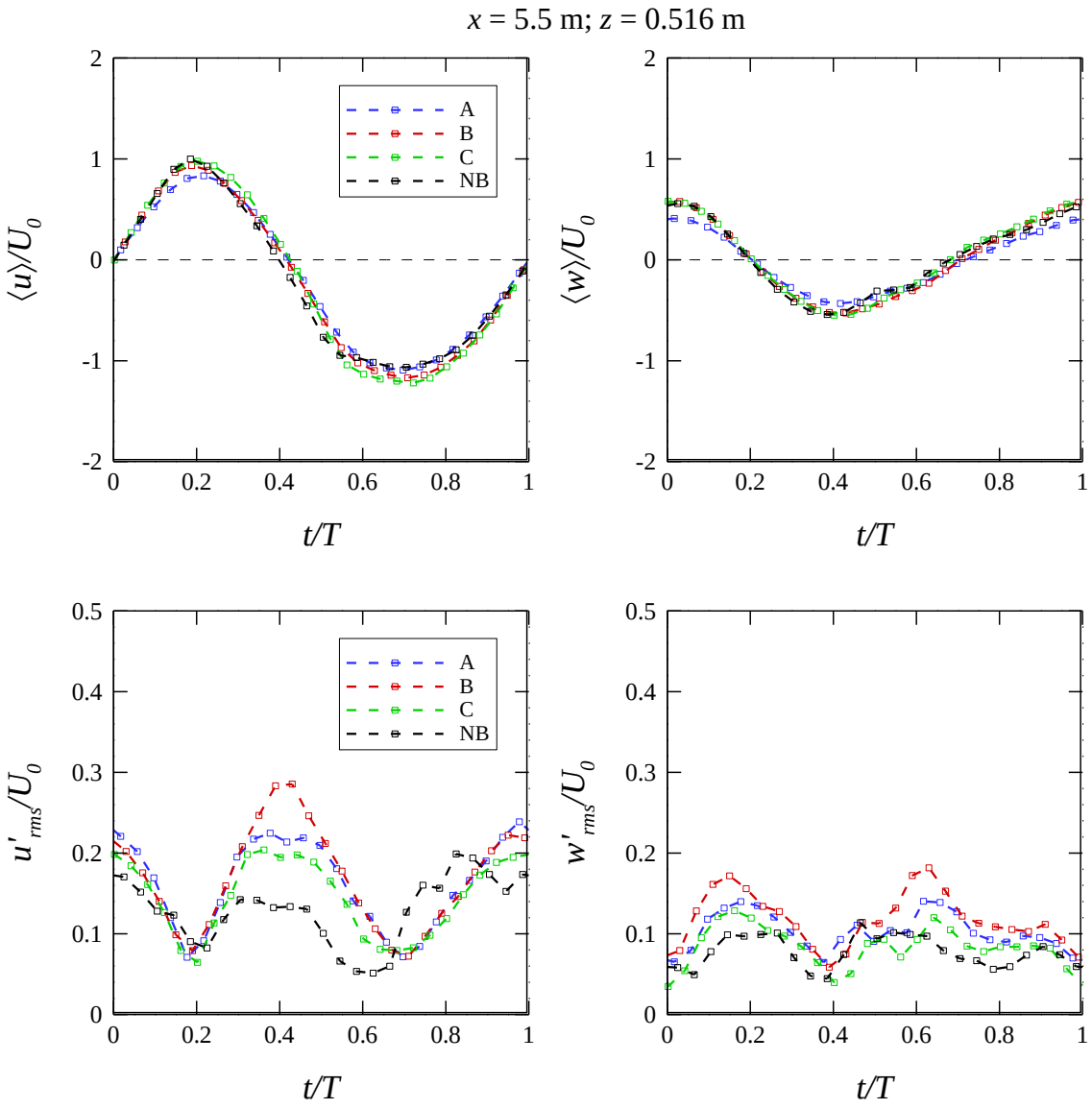

Fig. 11. Top: Phase-averaged longitudinal $\langle u \rangle$ (left) and vertical $\langle w \rangle$ (right) components of the velocity over one wave period at point x = 5.5 and z = 0.516 [m]; Bottom: RMS of the longitudinal u'_{rms} (left) and vertical w'_{rms} (right) components of the velocity at point x = 5.5 and z = 0.516 [m].

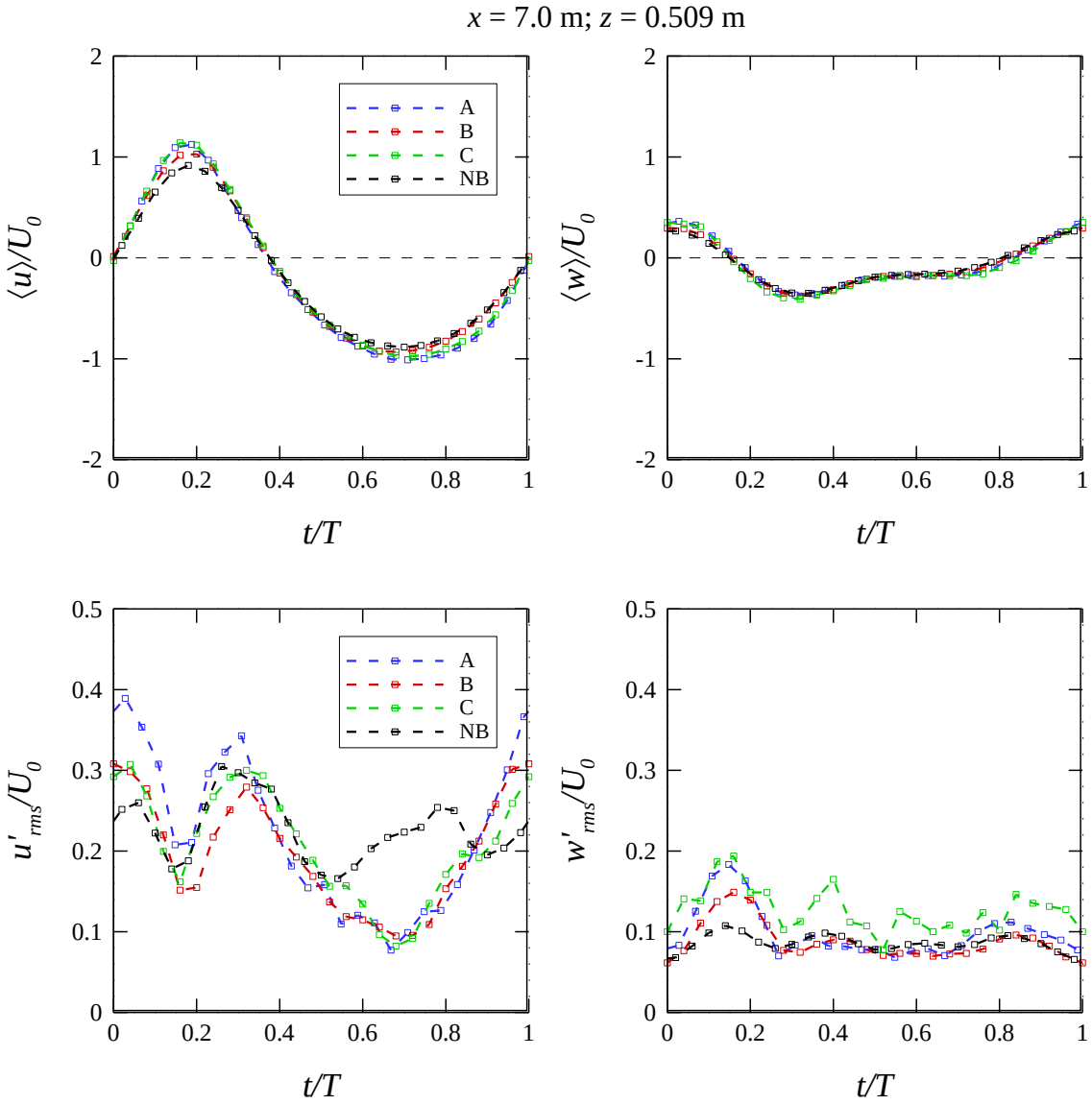

Fig. 12. Top: Phase-averaged longitudinal $\langle u \rangle$ (left) and vertical $\langle w \rangle$ (right) components of the velocity over one wave period at point x = 7.0 and z = 0.509 [m]; Bottom: RMS of the longitudinal u'_{rms} (left) and vertical w'_{rms} (right) components of the velocity at point x = 7.0 and z = 0.509 [m].

The vertical profiles of $\langle u \rangle$ and u'_{rms} at both sections x = 5.5 and x = 7.0 [m] are represented in Fig. 13 and Fig. 14, respectively. The same is presented in Fig. 15 and Fig. 16 for $\langle w \rangle$ and w'_{rms} for both vertical profiles. The vertical location of the flume bottom at the section of the vertical profile is z_0. The phase-average of the longitudinal and vertical components of the velocity show that, for both vertical profiles at x = 5.5 and x = 7.0 [m], there is not a specific trend that is observed from Fig. 13 to Fig. 16. However, the vertical profiles of u'_{rms} show that, for x = 5.5 and x = 7.0 [m], the NB case systematically presents lower values along the water column when compared with the air bubble curtain cases. For the case A, the vertical profile of u'_{rms} at x = 7.0 [m] (Fig. 14) presents consistently higher values when comparing with the other cases. For the vertical profiles at x = 5.5 [m] (Fig. 13) the three types of air bubble curtains (A, B and C) exchange the highest values along the water column, only showing smaller values for the case without air bubble curtain (NB).

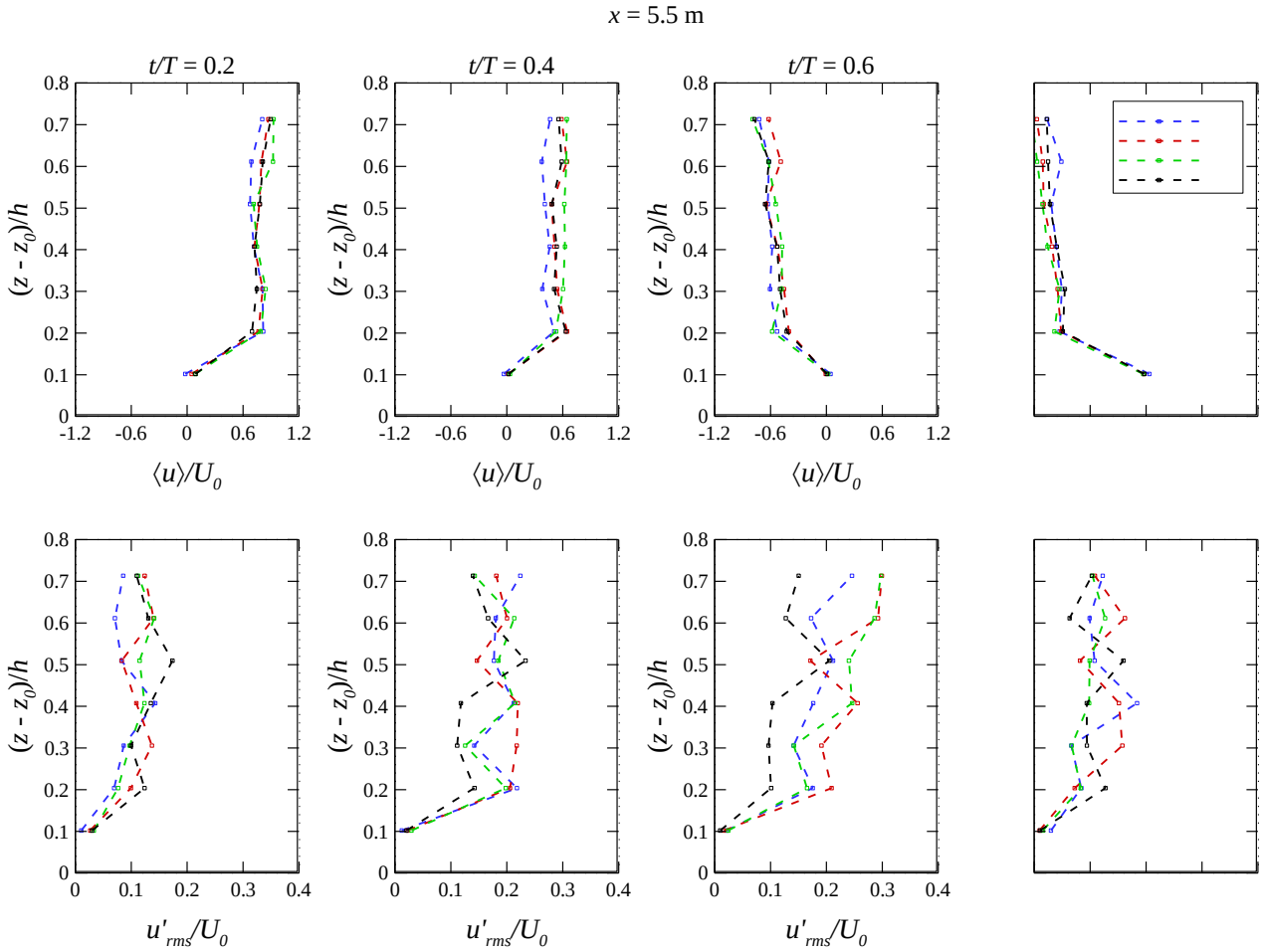

Fig. 13. Section x = 5.5 [m]. Top: Vertical profiles of the phase-averaged longitudinal component of the velocity ($\langle u \rangle$) at t/T = 0.2, 0.4, 0.6 and 0.8; Bottom: Vertical profiles of u'_{rms} at t/T = 0.2, 0.4, 0.6 and 0.8.

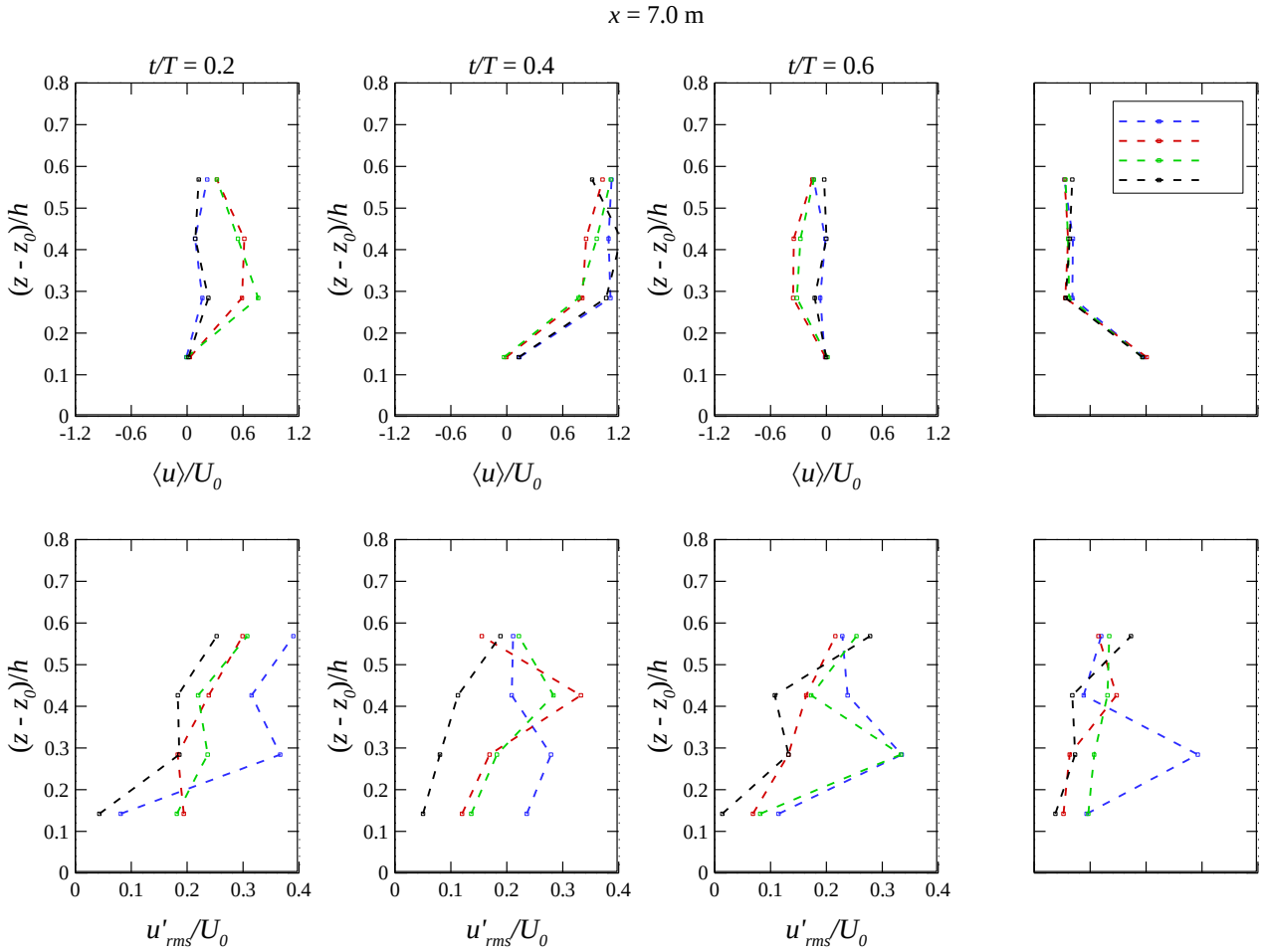

Fig. 14. Section x = 7.0 [m]. Top: Vertical profiles of the phase-averaged longitudinal component of the velocity ($\langle u \rangle$) at t/T = 0.2, 0.4, 0.6 and 0.8; Bottom: Vertical profiles of u'_{rms} at t/T = 0.2, 0.4, 0.6 and 0.8.

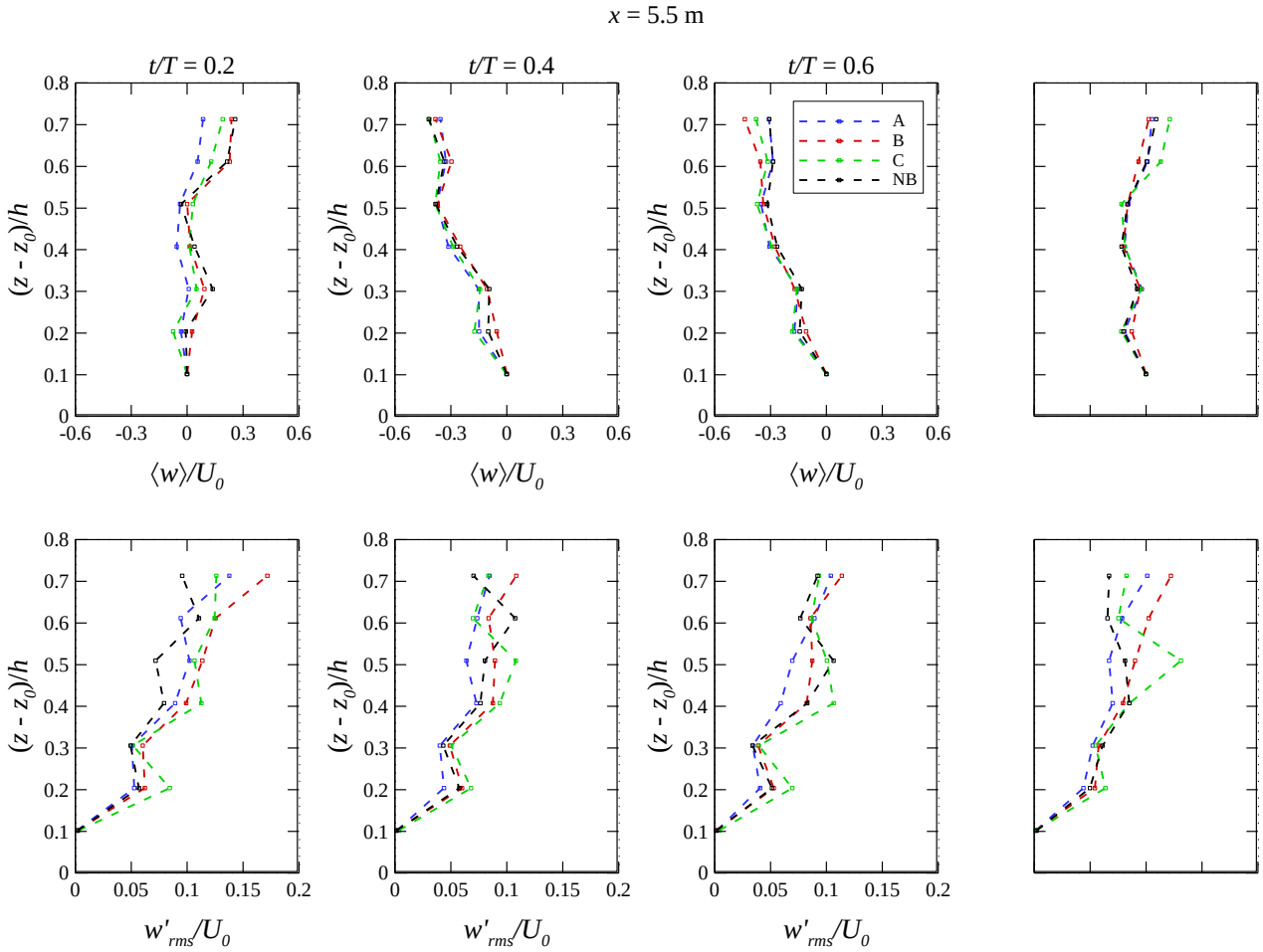

Fig. 15. Section x = 5.5 [m]. Top: Vertical profiles of the phase-averaged longitudinal component of the velocity ($\langle w \rangle$) at t/T = 0.2, 0.4, 0.6 and 0.8; Bottom: Vertical profiles of w'_{rms} at t/T = 0.2, 0.4, 0.6 and 0.8.

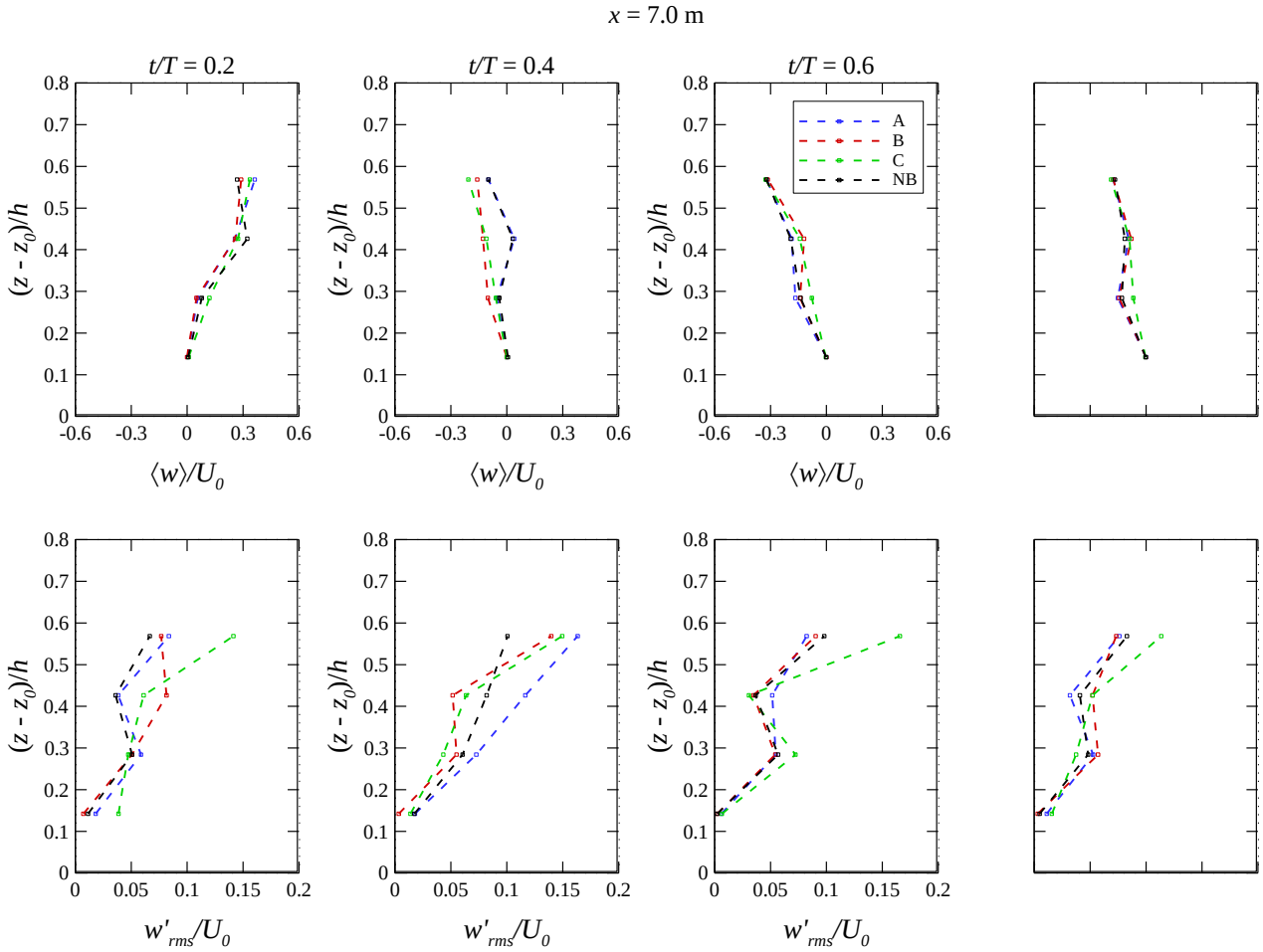

Fig. 16. Section x = 7.0 [m]. Top: Vertical profiles of the phase-averaged longitudinal component of the velocity ($\langle w \rangle$) at t/T = 0.2, 0.4, 0.6 and 0.8; Bottom: Vertical profiles of w'_{rms} at t/T = 0.2, 0.4, 0.6 and 0.8.

3.3. Turbulence. For the turbulence analysis, the turbulence intensity, I, in each direction was calculated for each measured point of the vertical profiles as:

$$I_x = \frac{\sqrt{\langle u' \rangle^2}}{U_0} \;;\; I_y = \frac{\sqrt{\langle v' \rangle^2}}{U_0} \;;\; I_z = \frac{\sqrt{\langle w' \rangle^2}}{U_0} \tag{5}$$

Also, the Reynolds shear stress $\langle u'w' \rangle$ and the turbulent kinetic energy k, given as:

$$k = \frac{1}{2}\left(u'^2 + v'^2 + w'^2\right) \tag{6}$$

The power spectra of velocity components were obtained by Fast Fourier Transform (FFT) technique. Fig. 17 shows for both measured vertical profiles (x = 5.5 and x = 7.0 [m]) of the three components of the turbulence intensity and the turbulent kinetic energy.

One can observe that the I_x for both sections (Fig. 17) shows a smaller turbulent intensity for the case without air bubble curtain (NB). At section x = 5.5 [m] the case B presents a vertical profile with larger values of I_x and at x = 7.0 [m] the case A that presents larger values. The vertical profiles of the turbulent kinetic energy show identical to I_x vertical profiles, due to the fact that u' presents larger values than the ones of v' and w', , where NB presents the smaller values. The Fig. 17 indicates that the turbulence for every test (A, B, C and NB) is not isotropic because $I_x \neq I_y \neq I_z$.

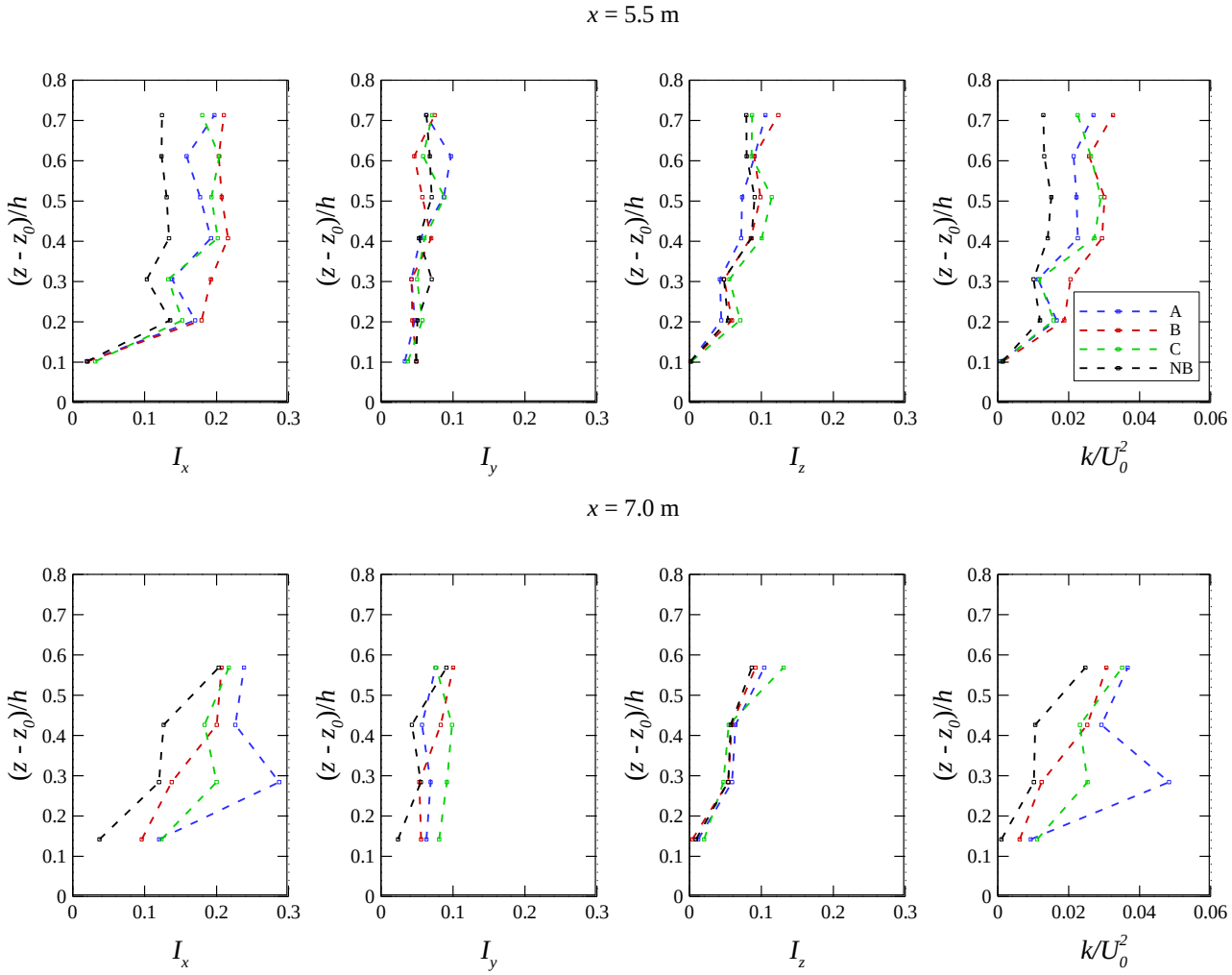

Fig. 17. Vertical profiles of the three components of the turbulence intensity (I_x, I_y, I_z) and the turbulent kinetic energy k/U_0^2 for both sections x = 5.5 and x = 7.0 m.

3.3. Power spectrum. Fig. 18 and Fig. 19 show the power spectra of u', v' and w' for two points in each of the sections x = 5.5 and x = 7.0 [m]. Gradients of approximately −5/3 (on the log-log scale), typical of isotropic (inertial-range) turbulence, and −3, typical of two-dimensional frozen turbulence are seen on the Fig. 18 and Fig. 19. The gradients of −5/3, occur down to a normalized frequency of 0.1. A background gradient close to −3 only appears to occur for case A at x =5.5 and x = 7.0 [m] (near the bed and free surface) where there are marked harmonics at frequencies greater than 0.1. This does not occur for the case NB at any position. The Nyquist filter frequency is about 10 Hz and random turbulence below this frequency is not accounted for in the Fourier analysis. Thus, the obtained turbulence quantities will only superimpose residual values of relatively high frequency (i.e., $f/f_0 > 10^{-2}$), not representative of all turbulence energy. Despite the approximately −5/3 gradients, we can observe from the turbulence intensity and turbulent kinetic energy that this residual turbulence is far from isotropic (Fig. 17).

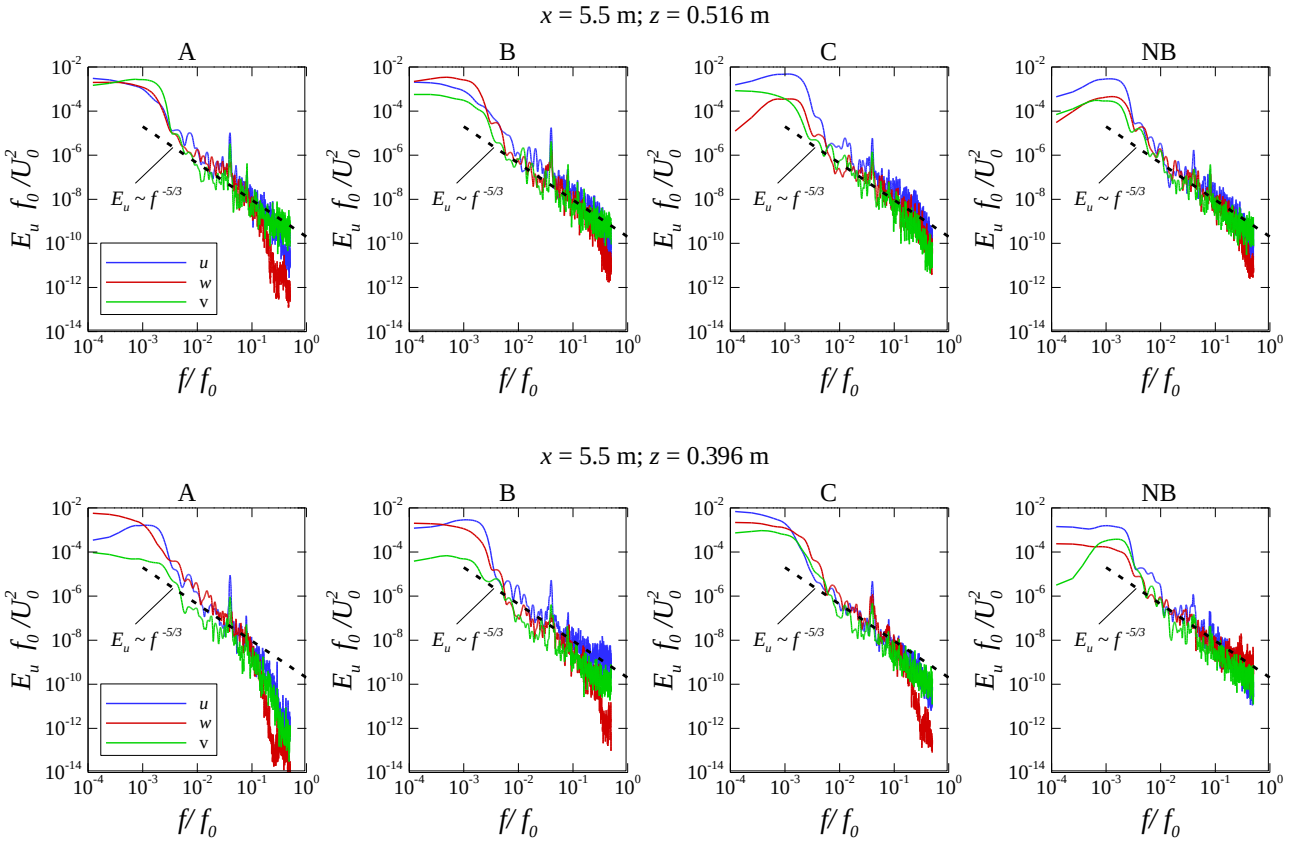

Fig. 18. Velocity spectra for section x = 5.5 [m] at locations z = 0.516 and z = 0.396 [m].

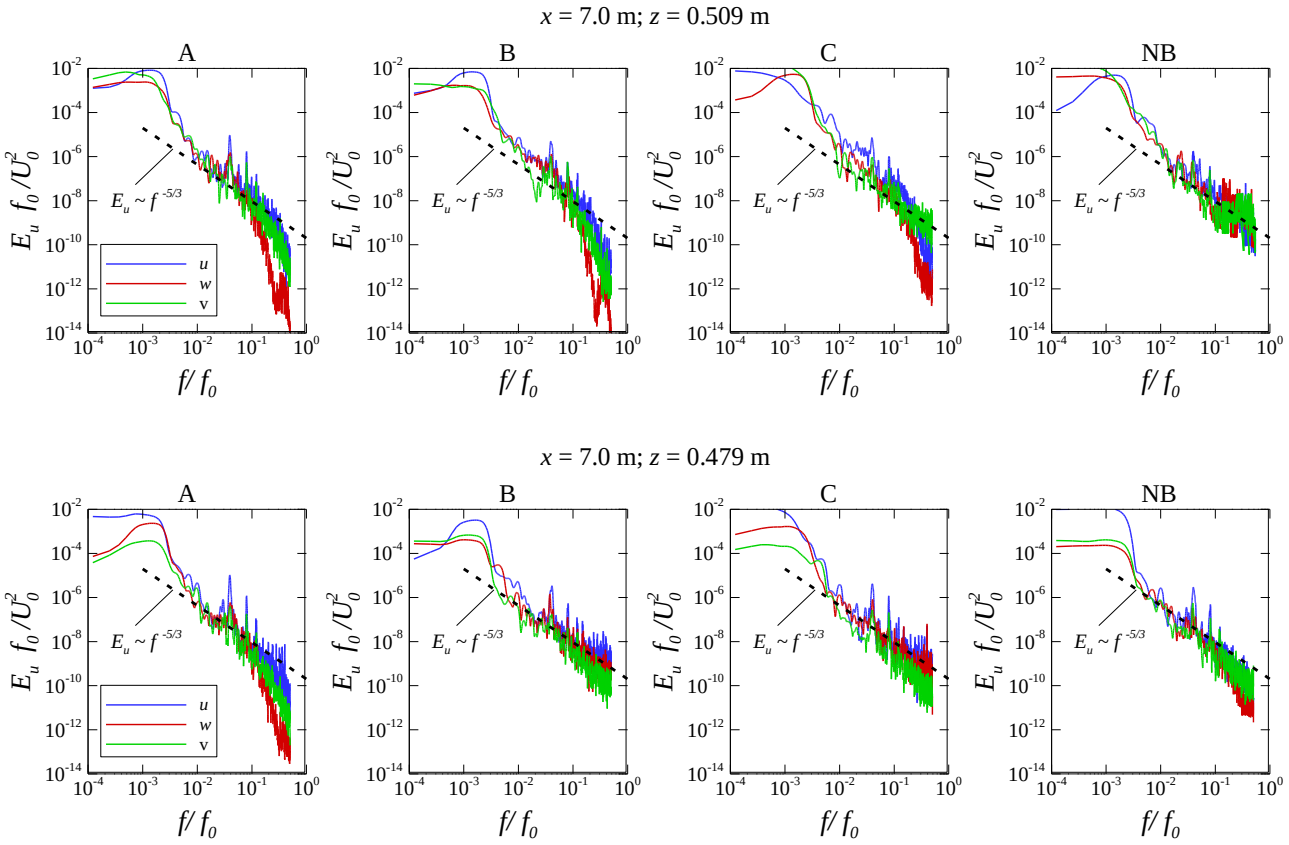

Fig. 19. Velocity spectra for section x = 7.0 [m] at locations z = 0.509 and z = 0.479 [m].

4. Results and Discussion

The effect of an air bubble curtain in a wave propagation flow field was investigated in a laboratory wave flume. The experimental tests embraced a set of different configurations for the air bubble curtains (A, B, and C) that were compared against the case without the air bubble curtain (NB). The three configurations were set by changing the number of air injection orifices and the thickness of the air bubble curtain. The measurements were made along the water column in two cross-shore locations downstream of the air bubble curtain.

Free surface elevations and flow velocities were measured and analyzed. Also, the turbulence and the power spectrum were investigated.

Regarding the free surface elevation data analysis, we observe that the case without air bubbles (NB) has shown greater amplitudes. This suggests that the air bubbles can slightly attenuate the free surface elevation. Moreover, the flow field generated by the air bubbles causes a more variable free surface elevation for the wave propagation, increasing the η'_{rms}.

Regarding the velocities, the root-mean-square (RMS) of *u*, *v* and *w* is also lower for the case without air bubbles (NB). The component *w* shows a clear increase with the air bubbles, and a larger difference for the cases where the air bubble curtain is thicker (A and B). The three components of the velocity are significantly affected by the tested air bubble curtains. The above conclusions are also reflected in the turbulence analysis where the turbulence intensity (*I*) is smaller for the case without air bubble curtain (NB). The cases with thicker air bubble curtains (A and B) exchange the highest turbulence intensities between both measuring sections. The turbulent kinetic energy shows also the same trend where the longitudinal component (u') is higher than the vertical and transverse components (v' and w').

The performed power spectra analysis shows that near the bed, and close to the free surface, the effect of the air bubble curtains is relevant for the energy distribution along the frequencies showing a clear difference when compared to the power spectrum curve of the case without air bubble curtain.

The two cases with thicker air bubble curtains (A and B) represent the cases that differ the most from the one without air bubbles (NB). The case C presents a lower effect on the flow field of a propagating wave.

The work here presented represents the first approach to investigate the effect of air bubble curtains in the wave flow field. This work shows that air bubble curtains can influence the wave field. Therefore, the results here presented confirm the need to investigate further the effect of the air bubbles in the flow field and to which extend can this technique be applied to solve real problems. Such as its capacity to change or block the flow field for coastal and offshore structure protection, sediment transport, or to protect environments from pollutants.

References

[1] H. Chanson, Air bubble entrainment in free surface turbulent shear flows, Academic Press, 2002.

[2] H. Chanson, Hydraulics of aerated flows: qui pro quo?, J. Hydr. Res., 51(3), 223-243, J. Hydraulic Research, vol. 51, no. 3, pp. 223–243, 2013.

[3] H. Chanson, S. Aoki, and A. Hoque, Scaling Bubble Entrainment And Dispersion In Vertical Circular Plunging Jet Flows: Freshwater Versus Seawater, in Proc. 5th Intl Conf. On Hydrodynamics ICHD2002, 2002.

[4] A. Hoque, Studies of water level rise by entrained air in the surf zone, Exp. Therm. Fluid Sci., vol. 32, no. 4, pp. 973–979, Feb. 2008, doi: 10.1016/j.expthermflusci.2007.11.003.

[5] A. Hoque and S. Aoki, Air entrainment and associated energy dissipation in steady and unsteady plunging jets at free surface, Appl. Ocean Res., vol. 30, no. 1, pp. 37–45, Feb. 2008, doi: 10.1016/j.apor.2008.03.004.

[6] K. Horikawa and C.-T. Kuo, A study on wave transformation inside surf zone, Proc. 10th Int. Conf. Coast. Eng. ASCE, vol. Vol. 1, pp. 217–233, 1966.

[7] D. T. Cox and S. Shin, Laboratory Measurements of Void Fraction and Turbulence in the Bore Region of Surf Zone Waves, J. Eng. Mech., vol. 129, pp. 1197–1205, 2003, doi: 10.1061/(ASCE)0733-9399(2003)129:10(1197).

[8] N. Mori and S. Kakuno, Aeration and bubble measurements of coastal breaking waves, Fluid Dyn. Res., vol. 40, no. 7–8, pp. 616–626, Jul. 2008, doi: 10.1016/j.fluiddyn.2007.12.013.

[9] C. E. Blenkinsopp and J. R. Chaplin, Void fraction measurements and scale effects in breaking waves in freshwater and seawater, Coast. Eng., vol. 58, no. 5, pp. 417–428, May 2011, doi: 10.1016/j.coastaleng.2010.12.006.

[10] V. Dugué, K. Blanckaert, Q. Chen, and A. J. Schleiss, Influencing flow patterns and bed morphology in open channels and rivers by means of an air-bubble screen, J. Hydraul. Eng., vol. 141, no. 2, pp. 1–13, 2015, doi: 10.1061/(ASCE)HY.1943-7900.0000946.

[11] Information on https://canadianpond.ca/air-bubble-curtains-bubble-tubing/

[12] U. S. A. Corps and O. F. Engineers, Sensory Deterrent Systems, no. April, pp. 1–8, 2012.

[13] Information on https://www.sintef.no/en/latest-news/fighting-oil-spills-with-air-bubbles-/

[14] Information on https://www.diversifiedpondsupplies.com/bubble-tubing-tm/bubble-curtain

[15] Information on https://flkeysaeration.com/bubble-curtains/

[16] Information on https://thegreatbubblebarrier.com/en/

[17] M. Brito, R. M. L. Ferreira, L. Teixeira, M. G. Neves and R. B. Canelas, Experimental investigation on the power capture of an oscillating wave surge converter in unidirectional waves, Renewable Energy, vol. 151, pp. 975-992, 2020, doi: 10.1016/j.renene.2019.11.094.

[18] G. Klopman, Vertical structure of the flow due to waves and currents". Delf Hydraulics Publication, Report H 840, 1994.

[19] F. C. K. Ting and J. T. Kirby, Observation of undertow and turbulence in a laboratory surf zone, Coast. Eng., vol. 24, no. 1–2, pp. 51–80, 1994, doi: 10.1016/0378-3839(94)90026-4.